ACS APPLIED MATERIALS & INTERFACES

Research Article

www.acsami.org

Mixed Matrix Membranes with Strengthened MOFs/Polymer Interfacial Interaction and Improved Membrane Performance

Rijia Lin,[†] Lei Ge,*[,†] Lei Hou,[†,‡] Ekaterina Strounina,[§] Victor Rudolph,[†] and Zhonghua Zhu*[,†]

[†]School of Chemical Engineering, The University of Queensland, Brisbane, Queensland 4072, Australia

[‡]Key Laboratory of Synthetic and Natural Functional Molecule Chemistry of the Ministry of Education, Northwest University, Xi'an, Shanxi 710069, P.R. China

[§]Centre for Advanced Imaging, The University of Queensland, Brisbane, Queensland 4072, Australia

Supporting Information

ABSTRACT: MOFs-based mixed matrix membranes (MMMs) have attracted extensive attention in recent years due to their potential high separation performance, the low cost, and good mechanical properties. However, it is still very challenging to achieve defect-free interface between micrometer-sized MOFs and a polymer matrix. In this study, $[Cd_2L(H_2O)]_2{\cdot}5H_2O$ (Cd-6F) synthesized using 4,4′-(hexafluoroisopropylidene)diphthalic anhydride (6FDA) as an organic ligand was introduced into the 6FDA-ODA polyimide matrix to achieve novel MOF MMMs. A specific interfacial interaction between MOF crystals and polymer chains was innovatively targeted and achieved through in situ polymerization procedure. The enhanced adhesion between MOF particles and polymer phase was observed, and the improved interfacial interaction between Cd-6F and the 6FDA-ODA polyimide matrix was confirmed by detailed characterizations including FTIR and NMR. In the meantime, the gas permeance and selectivity of the MMMs are strongly dependent on their morphology. The MMM derived from in situ polymerization presents excellent interfaces between micrometer-sized MOF crystals and the polymer matrix, resulting in increased permeability and selectivity. The strategy shown here can be further utilized to select the MOF/polymer pair, eliminate interfacial voids, and improve membrane separation performance of MOFs-based MMMs.

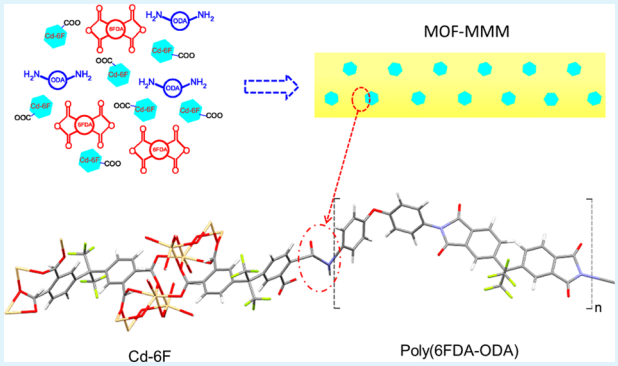

KEYWORDS: *metal organic frameworks, mixed matrix membranes, interfacial interaction, membrane morphology, gas separation*

1. INTRODUCTION

Gas separation continues to be an active area of research, and membrane technology has been found far superior to the conventional separation method, for its high energy efficiency, low production cost, and inappreciable environmental impact.[1−3] Nonetheless, most of the conventional polymer membranes are restricted to the limit of trade-off between permeability and selectivity,[4,5] for instance, high selectivity is always achieved at the cost of low permeability. One effective treatment is to introduce inorganic fillers such as zeolites,[6,7] carbon nanotubes,[8,9] carbon molecular sieves,[10,11] and mesoporous silica[12] into a polymer matrix to obtain mixed matrix membranes (MMMs). The selection of inorganic fillers is commensurate with the importance of the polymer matrix, which depends not only on the separation performance of inorganic particles but also on the compatibility with the polymer matrix.

Metal organic frameworks (MOFs), novel hybrid materials consisting of organic and inorganic moieties in crystalline lattices, have many characteristics favorable towards use as filler embeded in MMMs.[13−16] Due to their large surface area, controllable porosity and high adsorption affinity,[17,18] it provides promising opportunities of developing novel MOF MMMs with outstanding permeability and selectivity. MOF MMMs show an impressive separation performance with the combination of molecular sieving effect of MOFs and common feature of polymers matrix, which can be an alternative approach to solve the trade-off problem of traditional polymer membranes. Moreover, the employment of MOFs in MMMs provides several potential advantages over other inorganic fillers; MOFs perform better compatibility with the polymer matrix since the organic linkers in MOFs can provide stronger interaction with polymer chains.[19]

Despite the promising perspectives, the production of MOFs-based membranes is still an on-going area of investigation. As the structure is heterogeneous, defects can be observed between MOFs and polymer matrix which may be the underlying reason for the deterioration of gas selectivity and integrity of membrane structure.[10,20,21] To achieve good interfacial morphology, the

Received: January 5, 2014
Accepted: March 26, 2014
Published: March 26, 2014

   dx.doi.org/10.1021/am500081e | ACS Appl. Mater. Interfaces 2014, 6, 5609−5618

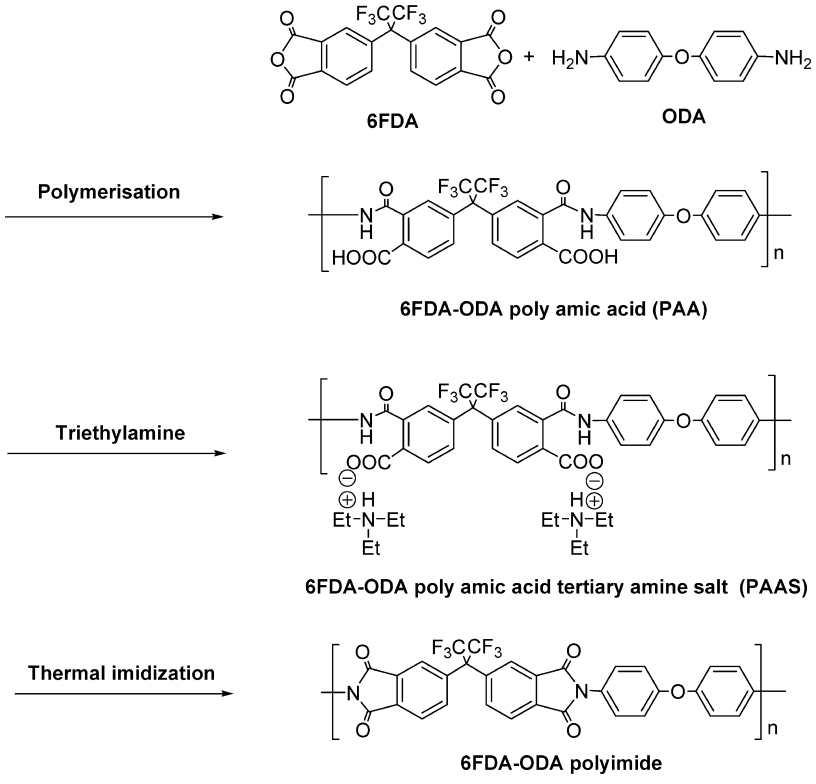

Figure 1. Multistaged of 6FDA-ODA poly(amic acid) salt and polyimide synthesis.

following needs to be considered: (1) proper selection of the MOF/polymer pair, (2) sufficient dispersion of inorganic phase in the polymer phase to avoid aggregation of particle, and (3) enhancement of interfacial interaction between inorganic phase and continuous phase. Amongst them, pair-wise selection is the basis for MMMs fabrication which is associated with affinity and compatibility between filler particles and polymer. Several experimental approaches have been proposed to produce MMMs with favorable interfacial property.[22−27] In general, the size of MOFs particles is preferable to be nano- or submicrometer (e.g. ZIF-8 and NH_2-MIL-5) in order to achieve strong interaction with the polymer matrix as well as good dispersion.[22−24,28−31] A void-free MMM with high gas separation performance was prepared by Bae et al. by applying as-synthesized submicrometer-sized ZIF-90 in fabrication of ZIF-90/6FDA-DAM.[31] On the other hand, the implement of micrometer-sized MOFs as fillets requires stronger interfacial adhesion which can be achieved through modification of MOFs and/or polymers. Functionalization of MOFs can improve the affinity between MOF linkers and polymer chains and also eliminate the formation of nonselective interfacial voids.[20,21] Another feasible way is tailoring MOFs by physical treatment. In our previous work, the size of Cu-BTC was reduced by using a facial sonication post-treatment, and the affinity between MOF and polymer is largely improved.[27] Compared to modification of MOFs, a polymer matrix can be improved by introducing a cross-linkable polymer (e.g. copolyimides) and solidifying it after the cast of MMMs[26] or surface cross-linking the MMMs with a cross-linking agent.[25]

Although numerous research has been conducted on MOF-based MMMs, the studies on the selection of the appropriate MOFs/polymer couples for targeting MOF/polymer interfacial controls are still limited. In this study, a specific MOF/polymer pair was chosen for the MMM fabrication with targeted interfacial interaction. For polymer selection, 4,4′-(hexafluoroisopropylidene)diphthalic anhydride-4,4′-oxydianiline (6FDA-ODA) polyimide was selected in this work due to its good combination of selectivity and permeability coefficients for CO_2/CH_4 separation.[32,33] As to the MOFs, $[Cd_2L(H_2O)]_2 \cdot 5H_2O$ (Cd-6F)[34,35] with high sorption selectivity of CO_2 over N_2 and CH_4 was chosen here to embed into the 6FDA-ODA polymer matrix. Particularly, Cd-6F was synthesized by using 4,4′-(hexafluoroisopropylidene)diphthalic anhydride (6FDA) as the organic linker which is also one of the monomers in the 6FDA-ODA synthesis. Targeted interfacial interaction was studied by controlling the in situ polymerization synthesis procedure. The MOFs MMMs morphology and membrane gas separation were also comprehensively investigated.

2. EXPERIMENTAL SECTION

2.1. Materials. 4,4′-(Hexafluoroisopropylidene)diphthalic anhydride (6FDA), oxydianiline (ODA), cadmium nitrate tetrahydrate, dimethylformamide (DMF), triethylamine, ethanol, and methyl ethyl ketone (MEK) were supplied by Sigma-Aldrich.

2.2. Cd-6F Crystals Synthesis. Cd-6F was synthesized based on a manner reported elsewhere.[34] 0.868 g of $Cd(NO_3)_2 \cdot 4H_2O$ and 0.616 g of 6FDA were mixed into 70 mL of a 50 vol %:50 vol % ethanol−water. Then the mixture was transferred into a Teflon-lined stainless steel autoclave, heated at 140 °C for 72 h, and cooled to room temperature at a rate of 0.1 °C/min. The colorless crystals product was filtered, washed with DMF, and dried at 80 °C in vacuum for 24 h.

2.3. Membrane Preparation. The procedures of pure 6FDA-ODA polyimide membrane preparation are shown in Figure 1. 6FDA-ODA polyimide was prepared by a three-step method similar to a work reported elsewhere.[36] **In step 1**, 1.00 g of ODA was dissolved into 10 mL of DMF. Once the ODA was fully dissolved, 2.22 g of 6FDA powder was added, followed by 5 mL of DMF. The mixture was stirred under nitrogen at room temperature for 3 h to form poly(amic acid) (PAA). **In step 2**, 1.7 mL of triethylamine and 3 mL of DMF were added slowly to the reaction mixture, which was stirred under nitrogen at room

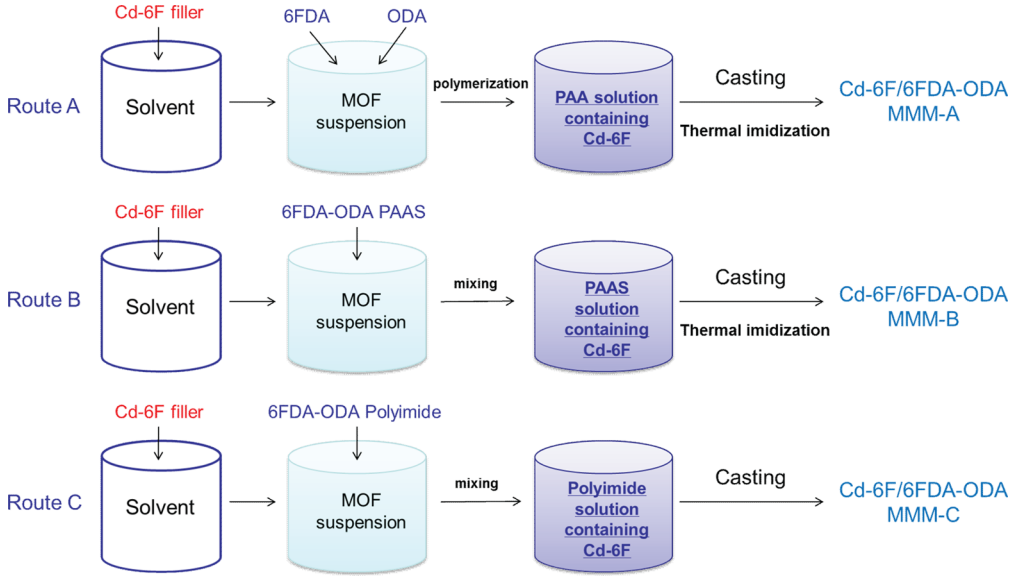

Figure 2. Schematic diagram of three different synthesis routes for Cd-6F based MMMs.

temperature for an additional 3 h. After that, poly(amic acid) tertiary amine salt (PAAS) was recovered by precipitating with a large amount of MEK, then washed by MEK, and dried at 50 °C for 24 h. **In step 3**, the polyimide film was obtained by thermal imidization of its PAAS. PAAS was dissolved in DMF (15 wt %) at room temperature and stirred for 6 h. The solution was cast onto a clean glass plate, followed by drying at 150 °C for 24 h in a vacuum oven.

Cd-6F based MMMs were prepared by incorporation of Cd-6F at each stage of polyimide synthesis, as shown in Figure 2. The derived MMMs from three different synthesis routes were marked as MMM-A, MMM-B, and MMM-C, respectively. Before embedding in mixed matrix membranes, the as-synthesised Cd-6F was ground into smaller and more uniform particles by ball milling (Fritsch, Pulverisette, Germany) for 15 min at a rotational speed of 750 rpm. For the films of type MMM-A, Cd-6F filler was dispersed in DMF and sonicated for 1-2 min before step 1 of the pure 6FDA-ODA membrane fabrication. Then the polymerization was carried on in the presence of MOF filler following step 1 and step 2 described above. After reacting with triethylamine, the filler suspension was directly cast onto a glass plate and heated at 150 °C for 24 h under vacuum to form the final product. In route B, Cd-6F was added into DMF, and the suspension was sonicated for 1-2 min before adding the PAAS obtained in step 2. The mixture was further stirred for 6 h and was cast onto a glass plate. MMM-B was obtained by thermal imidization of PAAS in the presence of Cd-6F at 150 °C for 24 h under vacuum. In route C, the solid PAAS was heated at 150 °C to prepare the 6FDA-ODA polyimide. Cd-6F was also dispersed in DMF and sonicated for 1-2 min. The 6FDA-ODA polyimide obtained by thermal imidization of PAAS was added followed by an additional 6 h stir. The resulting mixture was cast and dried at 150 °C for 24 h under vacuum to form MMM-C. The loadings of Cd-6F in composite membranes were calculated by eq 1

$$\phi = \frac{m_{\text{Cd-6F}}}{m_{\text{Cd-6F}} + m_{\text{6FDA-ODA polyimide}}} \quad (1)$$

where $m_{\text{Cd-6F}}$ and $m_{\text{6FDA-ODA polyimide}}$ are the mass of Cd-6F and 6FDA-ODA after imidization in the MMMs, respectively.

In order to investigate the interaction between Cd-6F and the polymer matrix, Cd-6F and ODA were mixed into DMF, and the suspension was stirred for 1 and 6 h, separately. The resulting Cd-6F was recovered by centrifugation and then washed by ethanol for several times to remove the remaining DMF. The resulting Cd-6F was dried at 80 °C in a vacuum oven.

2.4. Characterization. The X-ray diffraction spectra (XRD) of Cd-6F and mixed matrix membranes were obtained with a Bruker Advanced X-ray Diffractometer (40 kV, 30 mA) with Cu Kα (λ= 0.15406 nm) radiation at a scanning rate of 1° min^{-1} from 5° to 50°. Infrared spectra were obtained with a Perkin Elmer Spectrum 100 spectrometer equipped with an attenuated total reflection (ATR) objective. All spectra were collected from 650 to 4000 cm^{-1} wavenumbers. The thermal stability of MMMs and the Cd−6F loadings were measured by a Perkin Elmer Instruments STA 6000 Thermo Gravimetric Analyser. All samples were heated under an air atmosphere at a uniform heating rate of 5 °C min^{-1} from 40 to 800 °C. The N_2 adsorption isotherms of Cd-6F were obtained with a Micromeritics TriStar II 3020 at 77 K, after degassing the sample at 150 °C for 24 h and 200 °C for 2 h. The corresponding specific surface area was analyzed using the Langmuir and BET theories at relative pressure (p/p^0) between 0.005 and 0.05. After N_2 adsorption, the samples were regenerated at 150 °C under a pressure of 10 mTorr until no further pressure drop was observed. Then, the adsorption isotherms of CO_2 and N_2 at 273 and 298 K were measured using the same instrument. The desorption isotherms of CO_2 and N_2 were obtained by gradually decreasing the system pressure. The adsorption selectivity of CO_2 to N_2 (S) is calculated according to the following equation

$$S = \frac{q_{CO2}/q_{N2}}{p_{CO2}/p_{N2}} \quad (2)$$

where S is the relative selectivity value, q is the amount of adsorbed gas (cm^3 g^{-1}), and p is the exact gas pressure (kPa).

The high pressure sorption of CO_2 and N_2 was tested in BEL-BG using a magnetic suspension balance (Rubotherm) with high accuracies. About 0.7 g of pure 6FDA-ODA or MMMs was degassed at 80 °C under vacuum for 2 to 4 h before adsorption. The particle size distributions of the Cd-6F after ball milling was measured by a Malvern Zetasizer with 0.2% Cd-6F in ethanol at 25 °C. The analysis was done using a general purpose model. The morphologies of the samples were obtained with a JEOL JSM6300 scanning electron microscope (SEM) at 5 kV. Solid-state NMR was performed on the Avance III spectrometer (Bruker), operating at 300.13 MHz for ^{1}H and 75.47 MHz for ^{13}C. Powdered material was placed in the 4 mm zirconium rotor with a Kel-F cap and rotated at 7 kHz. The CPMAS technique with a 1 ms cross-polarization time was employed. The usual parameters included a 42 ms acquisition time with a sweep width of 40 kHz and a recycling delay of 3 s; 2K data points were collected. High-power decoupling was applied using the tppm15 scheme. X-ray photoelectron spectroscopy (XPS) was performed on a PHI-560 ESCA (Perkin Elmer) using a non-monochromatic Mg Kα excitation source at 15 kV. The C 1s peak position was set to 284.6 eV and taken as an internal standard.

dx.doi.org/10.1021/am500081e | ACS Appl. Mater. Interfaces 2014, 6, 5609−5618

2.5. Permeation Test. The variable feed pressure and the constant volume permeation system were used to measure the gas permeation of pure 6FDA-ODA and MMMs, as described elsewhere.[9] The membranes were held under vacuum for approximately 5 min to achieve a steady state before being exposed to the selected gas at a specific pressure. Before switching to the feed gas, the membrane has to be degassed for some time to ensure the complete desorb of initial permeate gas. The permeation coefficient is calculated using the following equation

$$P = \frac{273.15 \times 10^{10}}{760AT} \frac{VL}{\frac{P_0 \times 76}{14.7}} \frac{dp}{dt} \quad (3)$$

where P is the permeation coefficient in barrer (1 barrer = 1×10^{-10} cm^3 (STP) cm cm^{-2} s^{-1} cm Hg^{-1}), A is the effective area of the membrane (cm^2), T is the absolute temperature (K), V is the dead-volume of the downstream chamber (cm^3), L is the membrane thickness (cm), P_0 is the feed pressure (psi), and dp/dt is the steady rate of pressure increase in the downstream side (mm Hg s^{-1}).

The ideal selectivity for two gases is determined as

$$\alpha = \frac{P_A}{P_B} \quad (4)$$

where P_A and P_B are the permeation coefficients of pure gas A and B, respectively.

3. RESULTS AND DISCUSSION

3.1. Synthesis and Characterization of Cd-6F. Figure 3 presents the XRD spectra Cd-6F and simulated structure diagram of Cd-6F. Based on the Cd-6F structural data,[34,35] the observed pattern shows high similarity to the simulated pattern, which confirms the formation of well-crystallined pure Cd-6F. Figure 4 shows the crystal morphology of the as-synthesized Cd-6F samples. The as-synthesized Cd-6F crystals consist of heterogeneous hexagonal-shaped crystals with various dimensions up to several mm long. In order to achieve more uniform distribution particles for the MMM fabrication, ball milling was used to reduce the size of the as-synthesized Cd-6F. After the ball mill treatment, the size of Cd-6F crystals becomes smaller (shown in Figure S1). The particle size distributions of ball mill-treated Cd-6F is also shown in Figure S2. The particles tend to be smaller and more homogeneously distributed compared to the as-synthesized sample Cd-6F, which matches well with the SEM observation (Figure S1).

Thermal gravimetric analysis (TGA) shows that Cd-6F remains stable below 250 °C, the weight loss can be assigned to the evacuation of solvent and coordinated H_2O (Figure S3), and the curve matches well with the previous report.[34] Noteworthy, the excellent thermal stability of Cd-6F can meet the requirement of membrane fabrication at the temperature of thermal imidization of the polymer (~150 °C). The nitrogen sorption isotherm of Cd-6F performed at 77 K is presented in Figure S4. The BET surface area and pore volume were summarized in Table S1. The results are consistent with the previous study.[34] The CO_2 and N_2 adsorption capacities of Cd-6F are depicted in Figure S5. The adsorption quantities of CO_2 and N_2 on the Cd-6F add up to 42.0 cm^3 g^{-1} and 5.11 cm^3 g^{-1}, respectively, at 111 kPa and 273 K. The adsorption capacity of CO_2 and N_2 decreases when the temperature increases to 298 K, which is similar to the previous work of Cd-6F.[34] The influence of temperature on the adsorption capability can be attributed to the decrease of maximum pore density (or pore capacity) with the increased molecular mobility during heating. More importantly, Cd-6F exhibits almost no uptake of N_2 (0.72 cm^3 g^{-1}) but a CO_2 uptake of up to 30.9 cm^3 g^{-1} at 298 K and ambient pressure. The relative CO_2/N_2 adsorption selectivity is as high as 42.89 at 298 K, 101 kPa, which is higher than that of most MOFs which are usually used in MMMs fabrication, such as Cu-BTC and MIL-53.[27,37] Therefore, with a combination of the promising sorption capacity and excellent selectivity at membrane operation temperature (298 K), Cd-6F can provide great potential in gas separation.

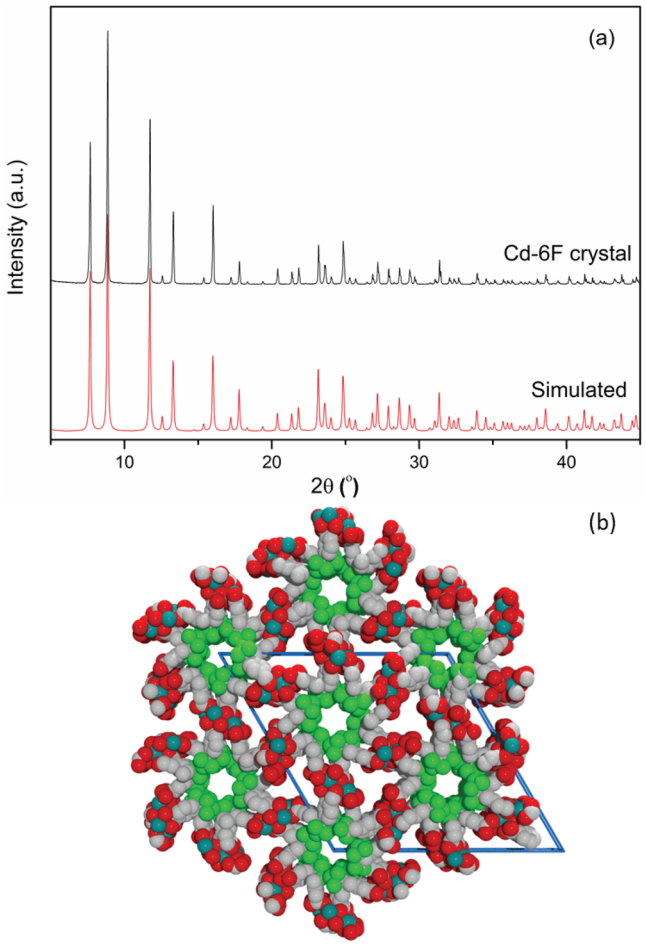

Figure 3. (a) XRDs spectra of as-synthesized Cd-6F and (b) projection view of the Cd-6F framework along the *c*-axis (red: O, white: C, green: F, cyan: Cd).

3.2. Characterization of Cd-6F Mixed Matrix Membranes. In order to check the phase structure of MMMs and the stability of incorporated Cd-6F, the XRD patterns of MMMs synthesized in three routes with the same MOF loading were examined and are shown in Figure S6, along with the pure 6FDA-ODA polyimide. The XRD pattern of pure 6FDA-ODA shows a broad peak from 10° to 22°, which is consistent with the reported XRD pattern for 6FDA-ODA in the literature.[38] The patterns of MMM-A, MMM-B, and MMM-C all display main reflection peaks of Cd-6F matching well with the Cd-6F XRD pattern in Figure 1, indicating that the membrane preparation procedures different routes do not change the crystallinity of Cd-6F.

The FTIR-ATR spectra of the MMMs are shown in Figure S7. As to Cd-6F, bands at 1547 cm^{-1} and 1529 cm^{-1} represent the asymmetric stretching vibrations of the carboxylate groups in 4,4′-(hexafluoroisopropylidene) diphthalate, while that at 1409 cm^{-1} is for the symmetric stretching vibrations. As to the pure 6FDA-ODA polyimide, bands at 1725 cm^{-1} are attributed to the asymmetric stretch of the carbonyl group (imide I band), peaks at 1785 cm^{-1} are assigned to the symmetric stretch of the

dx.doi.org/10.1021/am500081e | ACS Appl. Mater. Interfaces 2014, 6, 5609−5618

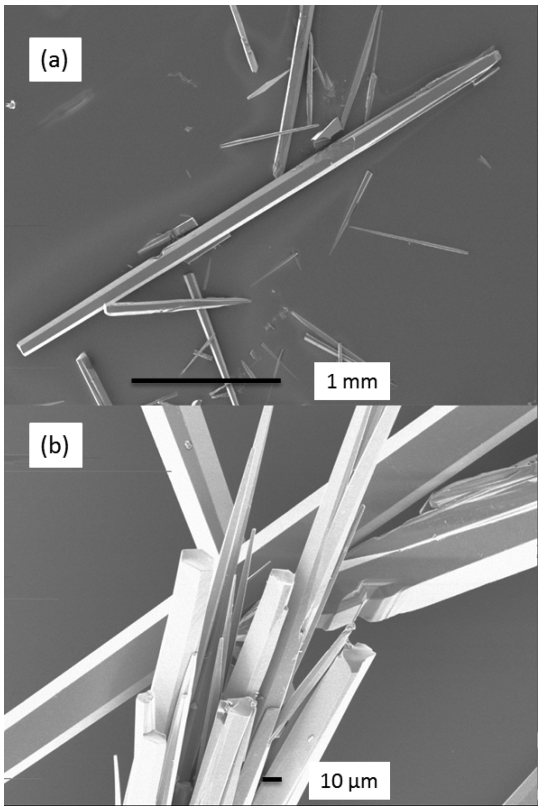

Figure 4. SEM images of as-synthesized Cd-6F crystals. a: low magnification; b: high magnification.

carbonyl group (imide II band), and bands at 1374 cm^{-1} correspond to the C−N stretch (imide rings). These characteristic peaks suggest that 6FDA-ODA membranes have imides functional groups.[36,38] For the Cd-6F/6FDA-ODA MMMs with a Cd-6F loading of 10 wt %, a weak band around 1550 cm^{-1} to 1530 cm^{-1} appears, indicating the presence of Cd-6F in MMMs. On the other hand, there is no obvious difference between the FTIR-ATR spectra of MMM-A, MMM-B, and MMM-C since all the MMMs have a similar chemical composition. Also signals of Cd-6F are overlapped by 6FDA-ODA peaks owing to the similar structure of 6FDA and relative low Cd-6F loading percentage in MMMs.

As to the MMMs, the interfacial morphology of polymer matrix and filler can dramatically affect the membrane integrity and overall transport properties. Improving the polymer−particle adhesion and eliminating the interface voids are critical for enhancing the separation performance of MMMs. Therefore, Cd-6F/6FDA-ODA was intentionally chosen as the MOF/polymer pair for the MMM fabrication in this study. A specific interfacial interaction was designed as described in Figure 5. The in situ polymerization was carried out in the presence of Cd-6F. Cd-6F crystals were dispersed into solvent to form a MOF suspension before adding ODA and 6FDA monomers and initializing the polymerization reaction. During the reaction, ODA not only reacts with 6FDA but also introduces a specific interaction between the $-COO^-$ on the surface of Cd-6F and the $-NH_2$ groups of the ODA monomer at the terminal of poly(6FDA-ODA) chains. Such a MOF/polymer contact was targeted to achieve remarkable MOF adhesion to the polymer matrix.

Figure 6 displays the SEM images of cross-section morphology of pure 6FDA-ODA and the corresponding MMMs synthesized from different procedures. As can be seen in Figures 6a and 6b, the cross-section of pure 6FDA-ODA polyimide is smooth and clean. In Figure 6c, d, the micrometer-sized Cd-6F crystals show excellent adhesion with the 6FDA-ODA polyimide in MMM-A, as indicated by arrows. No interfacial gaps are observed between Cd-6F and the polymer. As to the MMM-B (Figure 6e, f) and MMM-C (Figure 6g, h), the interface between Cd-6F and the polymer is clearly worse than that of the MMM-A. Some voids and poor adhesion at the MOF−polymer interface are observed, as indicated by circles. Therefore, different fabrication procedures play crucial roles on the morphology of Cd-6F/6FDA-ODA MMMs. The good compatibility with Cd-6F/6FDA-ODA in MMM-A can be explained by two main reasons: (1) Cd-6F was dispersed in the solvent before the polymerization reaction, and the reaction was carried out in the presence of Cd-6F. (2) There is a specific interfacial interaction between Cd-6F and the 6FDA-ODA polyimide under the condition of route A.

In order to investigate the interaction between Cd-6F and 6FDA, an intended experiment was carried out by mixing Cd-6F with ODA in DMF solution for several hours without 6FDA. The ethanol washed Cd-6F powder was characterized by FTIR, as shown in Figure 7. In the spectrum of ODA, the adsorptions at 815 cm^{-1}, 1620 cm^{-1}, and around 3350 cm^{-1} are corresponding to N−H of primary amine groups. The 1495 cm^{-1} peak in the ODA spectrum can be assigned to C═C ring stretching. The peak at 1212 cm^{-1} indicates the Ar−O−Ar stretching. After reacting Cd-6F with ODA, a weak band at 1651 cm^{-1} appeared, which should be ascribed to the C═O stretching vibration of amide. It is obvious that the peak intensity increased with the increase of reaction duration. On the other hand, peaks around 1620 and 3350 cm^{-1} in the ODA spectrum weaken in the Cd-6F-ODA spectrum. This is because that the primary amine groups $-NH_2$ in ODA are transformed into secondary amine groups −NH− after reacting with Cd-6F. The −NH− adsorption is relatively weak around 1620 and 3350 cm^{-1}; these peaks in Cd-6F-ODA spectra will become not obvious after the interfacial reaction. These results indicate that Cd-6F could interact with ODA by generating−NH−CO− groups, and more −NH−CO− groups can be formed on the surface of Cd-6F with prolonging the reaction time.

^{13}C solid-state NMR was used to further confirm the interaction between Cd-6F and the ODA monomer, as shown in Figure 8. Compared with the pattern of pure Cd-6F, a new peak at 165 ppm appeared (the red square in Figure 8a), which can be assigned to C═O emphasized in the red square in Figure 8b.[39,40] This result agrees well with the FTIR test in Figure 7.

XPS was also applied to check the interaction between Cd-6F and ODA, and the N 1s high resolution scan is shown in Figure S8. In the pattern of Cd-6F reacting with ODA, the N 1s peak around 398-401 eV should be assigned to the nitrogen of ODA, which indicated that the existence of ODA reacted on the surface of Cd-6F. Chemical compositions of Cd-6F before and after reacting with ODA were further characterized by element analysis. As it can be seen in Table S2, after reacting with ODA for 1 h, only 0.52 wt % of nitrogen on ODA treated Cd-6F was observed from element analysis. Since the Cd-6F crystal does not contain N, the measured nitrogen signals can only be attributed to the amino group of ODA. By prolonging the reaction time, an increment in the nitrogen content of ODA treated Cd-6F was acquired (0.71 wt %), indicating the enhancement of the interfacial interaction between more ODA and Cd-6F.

In IR and NMR results, the new C═O bond can be observed after the interfacial reaction between Cd-6F and ODA. Also the

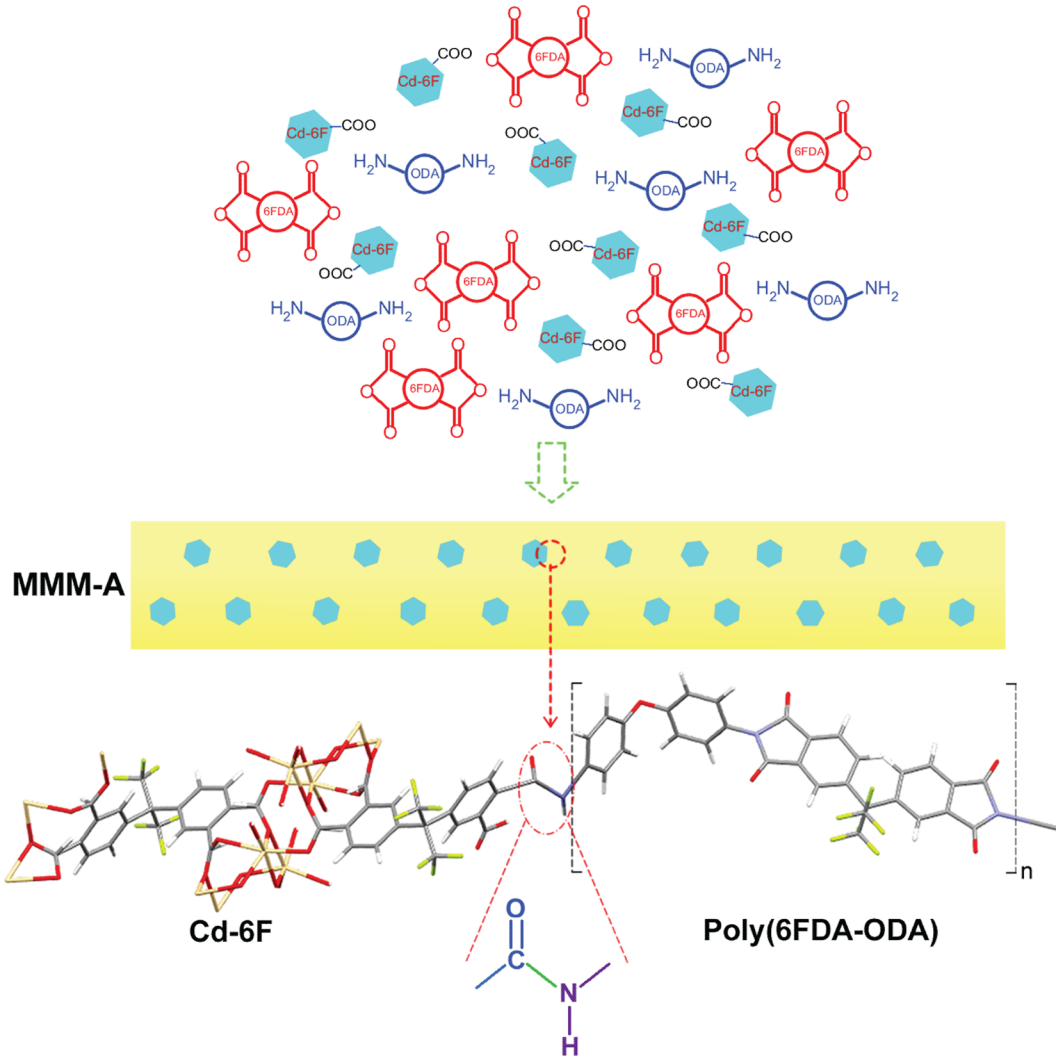

Figure 5. Diagram of designed interaction between Cd-6F and 6FDA-ODA in MMM-A.

1620 and 3350 cm^{-1} peaks in the IR spectrum of ODA become weakened in the IR spectrum of Cd-6F-ODA, which should be due to the change from primary amine groups $-NH_2$ to secondary amine groups −NH−. Both XPS and element analysis (Figure S8 and Table S2) reveal that the new bonds containing N are formed on the Cd-6F surface. Based on the above results, the interfacial interaction between Cd-6F and ODA by generating −NH−CO− groups can be concluded. During the in situ polymerization, the $-NH_2$ groups of the ODA monomer at the terminal of poly(6FDA-ODA) chains could have interaction with Cd-6F crystals, leading to the improved adhesion of the MOF/polymer in MMM-A. Meantime, the introduced interfacial interaction does not affect the structure of Cd-6F, and most of the Cd-6F crystals remain the same crystal structure as shown in the XRD spectra of MMM-A (Figure S6). This result demonstrates that the interaction between Cd-6F crystals and the polymer monomer may only occur on the surface of Cd-6F by reacting uncoordinated $-COO^-$ and $-NH_2$ groups. As a whole, the targeted MOF/polymer interface interaction can benefit the elimination of interfacial voids and enhance MOF/polymer adhesion without sacrificing MOFs structure stability.

3.3. Gas Permeation of Cd-6F Mixed Matrix Membranes. The ideal gas separation performance of pure 6FDA-ODA and MMMs with Cd-6F incorporation was measured. Figure 9 shows the gas permeability and selectivity at 25 °C and 2 atm feed gas pressure. Averaged values were calculated from no less than three permeation tests over each membrane (20−40 μm). As to the pure 6FDA-ODA, the gas permeation fluxes of CO_2, N_2, and CH_4 are 20.6, 0.78, and 0.62 barrer, respectively. The CO_2/N_2 and CO_2/CH_4 selectivity are 26.4 and 33.1, respectively. These results are consistent with the published values of the 6FDA-ODA membrane.[36] All the derived Cd-6F MMMs present higher gas permeability compared to the neat 6FDA-ODA polyimide membrane. It has been shown that inorganic particles could disrupt the polymer chain packing and create more free volume, resulting in the increase of the gas diffusivity as well as the permeability of the membrane.[41,42] Therefore, the increment of gas permeability of Cd-6F MMMs in this study can be attributed to the larger free volume introduced by incorporation of Cd-6F particles. On the other hand, even with the same MOF loading percentage, the ideal selectivity of the MMMs varies with the membrane synthesis procedures. Compared to the pure 6FDA-ODA polyimide membrane, MMM-A shows both higher permeability fluxes and selectivity values: CO_2 permeability of 37.8 barrer with a CO_2/N_2 selectivity of 35.1, and CO_2/CH_4 selectivity of 44.8, as expected from the good MOFs/polymer compatibility resulted from the targeted interfacial interaction. Specifically, the tight MOF/polymer

dx.doi.org/10.1021/am500081e | ACS Appl. Mater. Interfaces 2014, 6, 5609−5618

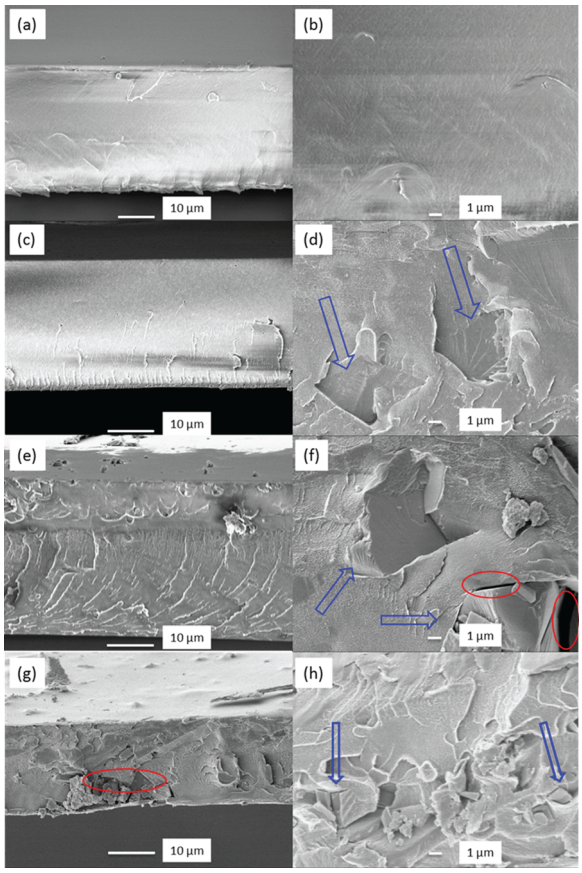

Figure 6. SEM images of pure 6FDA-ODA (a, b), MMM-A (c, d), MMM-B (e, f), and MMM-C (g, h). Arrows point to the MOF crystals embedded in polymer matrix. Circles indicate defects and voids between MOF and polymer matrix. The Cd-6F content of all the membranes is 10 wt %.

interface in MMM-A can eliminate the unselective gas diffusion through interfacial voids. In contrast to MMM-A from in situ polymerization, MMM-B and MMM-C exhibit much lower ideal selectivity values than that of the pure polymer, owing to the poor contact between MOF and polymer matrix as shown in Figure 6. Especially for MMM-C, though this membrane fabrication process is quite common for most MMMs, obtaining a good MOF/polymer interface is very challenging by incorporating a microsized filler if the MOF/polymer interaction cannot be built. In this case, the gas separation performance will be deteriorated with the existence of interfacial voids. Therefore, in order to achieve a satisfactory separation performance in the MMMs with microsized MOFs, the polymer/MOF pair should be carefully chosen, and the specific MOF/polymer interaction must be introduced through controlling the synthesis procedures and conditions.

In order to investigate the gas solubility difference between the pure 6FDA-ODA membrane and MMM-A, the membrane gas sorption was measured at a pressure up to 30 bar. Based on the solution-diffusion model, the penetrants need to dissolve in the membrane materials before diffusing through the membrane under the pressure gradient.[43] Figure S9 displays the CO_2 and N_2 adsorption results of 6FDA-ODA and MMM-A. The adsorption amount of CO_2 is much higher than that of N_2 in both membranes, which indicates these membranes have higher solubility of CO_2. As shown in Figure S9, after the introduction of Cd-6F, the sorption capacity of CO_2 rises slightly, while N_2 sorption drops. The reduction of the N_2 sorption amount can be attributed to the high CO_2/N_2 selectivity of Cd-6F. On the other hand, the gas sorption isotherms exhibit nonlinear pressure dependence, which is characteristic of the dual-mode sorption consisting of Henry's law sorption in the equilibrium region and Langmuir-type sorption in the nonequilibrium region.[44] The former is related to the dissolution of gases into the dense equilibrium structure of rubbery polymers, while the latter corresponds to the sorption on the holes or "microvoids" from the nonequilibrium nature of glassy polymers. The dual-mode sorption model is expressed by[45]

$$C = C_D + C_H = k_D p + \frac{C'_H b_p}{1 + b_p} \quad (5)$$

where C is the total gas concentration in a glassy polymer, C_D is the gas concentration based on Henry's law sorption, C_H is the gas concentration based on Langmuir sorption, k_D is the Henry's law coefficient, and b and C'_H are the hole affinity parameter and the capacity parameter, respectively, in the Langmuir model.

The measured CO_2 and N_2 sorption data can be well fitted by the dual-mode sorption model (Figure S10). The derived parameters are shown in Table S3. k_D represents the penetrant dissolved in the polymer matrix at equilibrium, C'_H shows the amount of the nonequilibrium excess free volume in the glassy state, and b characterizes the sorption affinity for a particular gas−polymer system.[46] The magnitude of these values all follows the order of $CO_2 > N_2$, the same as the gas condensability order. For CO_2 sorption, all parameters of the MMM-A have slight increments compared to those of the pure 6FDA-ODA membrane, which can be observed in Table S3. Cd-6F can disrupt the polymer chain packing to increase the free volume, resulting in the increment of C'_H. With introducing Cd-6F into 6FDA-ODA, the solubility and the sorption affinity of the membrane for CO_2 can be increased, reflecting on the increments of k_D and b. However, the reduction of k_D and b was observed for N_2. This can be due to the low adsorption abilities of Cd-6F for N_2. Cd-6F exhibits very low uptake of N_2 (0.72 $cm^3\ g^{-1}$) at 298 K and ambient pressure (Figure S5), leading to weaken the solubility and sorption affinity of N_2 (decrease of k_D and b). The increased k_D and b value of CO_2 and the decreased k_D and b value of N_2 indicate that more CO_2 and less N_2 can dissolve in MMMs by introducing Cd-6F into 6FDA-ODA. Combining these sorption results with the gas permeation test of MMM-A, the increase of permeability can be attributed to the increment of C'_H value owing to the increasing free volume created by the Cd-6F introduction. The enhanced solubility difference and selectivity for CO_2 over N_2 can be assigned to the opposite changing direction of k_D and b values for CO_2 and N_2 after the introduction of Cd-6F. As a whole, the improvement of membrane performance can be attributed to the increase of both diffusivity and solubility of CO_2.

4. CONCLUSIONS

In order to optimize the MOFs/polymer interface in the 6FDA-ODA polyimide matrix, Cd-6F synthesized from the 6FDA ligand was chosen as the MMM filler and the in situ polymerization process was used to tailor the interfacial interaction in this novel Cd-6F/6FDA-ODA MMMs. By controlling the in situ 6FDA-ODA polymerization procedure with the existence of Cd-6F, a specific interaction between the uncoordinated $-COO^-$ on the surface of Cd-6F and the $-NH_2$ groups of the ODA monomer at the terminal of poly(6FDA-

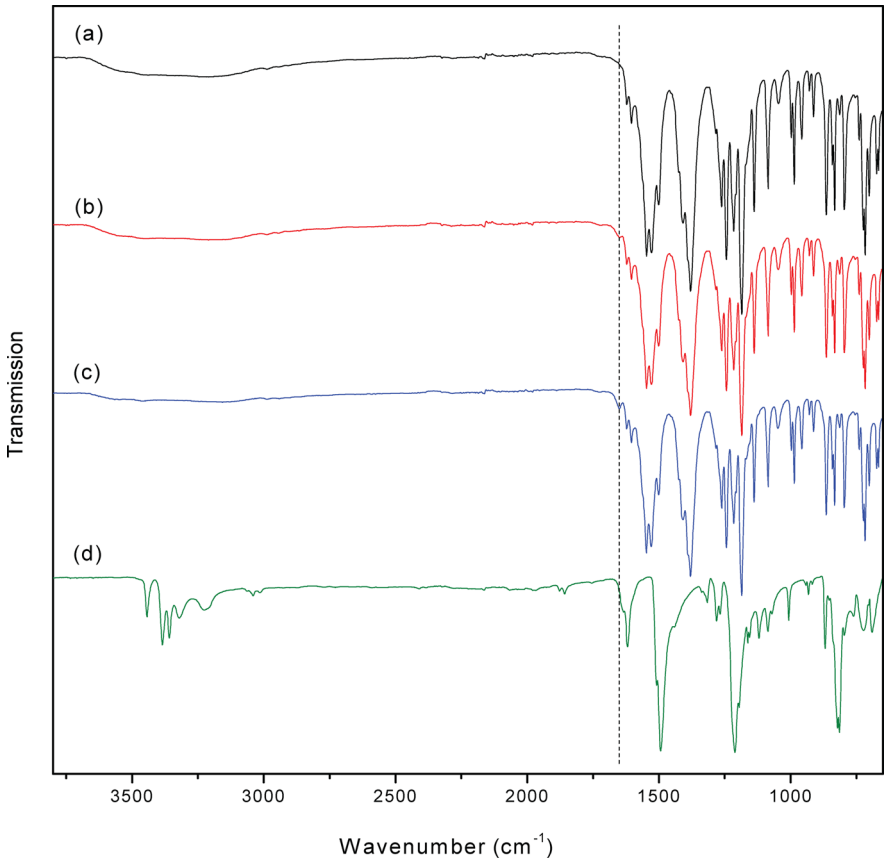

Figure 7. FTIR-ATR spectra of pure Cd-6F (a), Cd-6F mixed with ODA for 1 h (b), Cd-6F mixed with ODA for 6 h (c), and ODA (d).

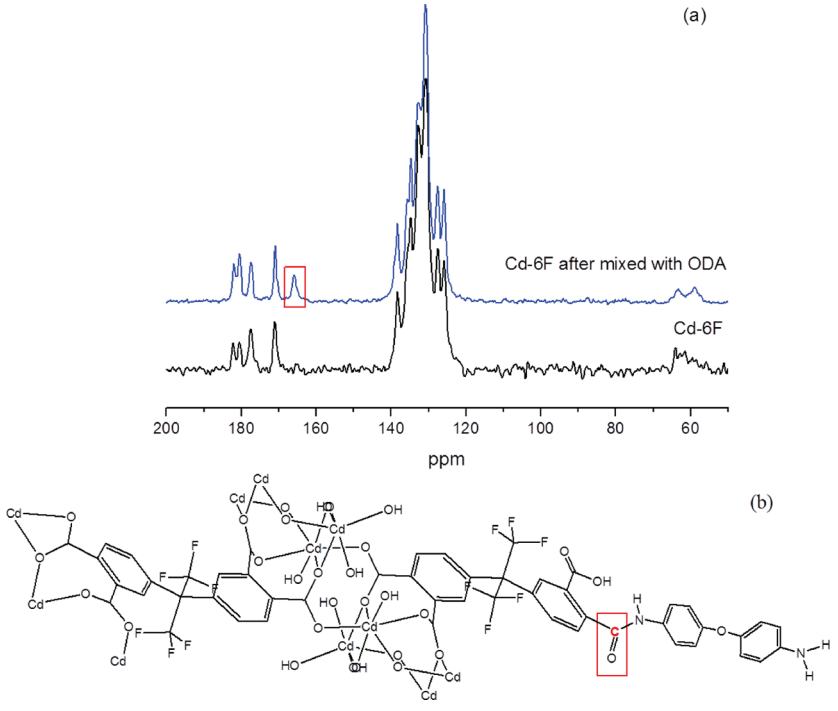

Figure 8. ^{13}C solid-state NMR spectra (a) of Cd-6F and Cd-6F mixed with ODA for 6 h and the structure of Cd-6F reacted with ODA (b).

ODA) chains has been introduced. As a result, Cd-6F in MMM-A derived from in situ polymerization of 6FDA-ODA with the existence of Cd-6F shows the best adhesion with the 6FDA-ODA matrix, while MMM-B and MMM-C synthesized from mixing Cd-6F and polymerized polymer display poor MOF/polymer interface. Both gas permeance and CO_2 selectivity of MMM-A are significantly improved compared to the pure 6FDA-ODA polymer membrane, while MMM-B and MMM-C show higher

dx.doi.org/10.1021/am500081e | ACS Appl. Mater. Interfaces 2014, 6, 5609−5618

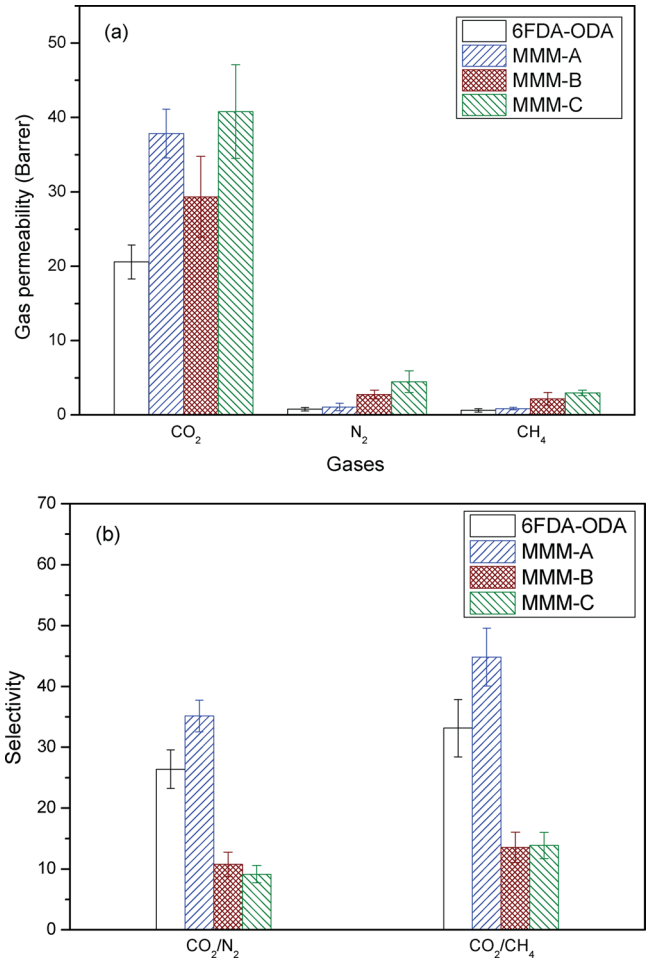

Figure 9. Gas permeability (a) and selectivity (b) of the pure 6FDA-ODA membrane and Cd-6F based MMMs.

gas permeation flux but lower CO_2 selectivity (over N_2 and CH_4) compared to MMM-A. The synthesis route and the MOF/polymer pair can be tailored for maximizing the membrane performance through optimizing the interaction between MOF fillers and polymer matrix. The membrane fabrication strategy we have shown here exploits a new guidance for the MOF/polymer pair selection and the interface manipulation in the fabrication of high performance MMMs by taking advantage of the organic linker on the surface of MOFs.

■ ASSOCIATED CONTENT

Ⓢ Supporting Information

SEM image and particle size distribution of ball mill-treated Cd-6F, TG profiles of Cd-6F, N_2 and CO_2 adsorption and desorption isotherms of Cd-6F, XRD patterns of MMMs, IR spectra of Cd-6F, 6FDA-ODA and MMMs, XPS spectra of Cd-6F and Cd-6F mixed with ODA, and high pressure CO_2 and N_2 sorption isotherms of Cd-6F and MMM-A. This material is available free of charge via the Internet at http://pubs.acs.org.

■ AUTHOR INFORMATION

Corresponding Authors

*Phone: +61 733653528. Fax: +61 733654199. E-mail: l.ge@uq.edu.au (L.G.).
*E-mail: z.zhu@uq.edu.au (Z.H.Z.).

Notes

The authors declare no competing financial interest.

■ ACKNOWLEDGMENTS

This work was financially supported by an Australian Research Council Discovery Project, and author Rijia Lin acknowledges additional financial support from a CSC scholarship from China.

■ REFERENCES

(1) Koros, B. Three Hundred Volumes. *J. Membr. Sci.* **2007**, *300*, 1−2.
(2) Alexander Stern, S. Polymers for Gas Separations: The Next Decade. *J. Membr. Sci.* **1994**, *94*, 1−65.
(3) Nasir, R.; Mukhtar, H.; Man, Z.; Mohshim, D. F. Material Advancements in Fabrication of Mixed-Matrix Membranes. *Chem. Eng. Technol.* **2013**, *36*, 717−727.
(4) Robeson, L. M. Correlation of Separation Factor versus Permeability for Polymeric Membranes. *J. Membr. Sci.* **1991**, *62*, 165−185.
(5) Robeson, L. M. The Upper Bound Revisited. *J. Membr. Sci.* **2008**, *320*, 390−400.
(6) Bastani, D.; Esmaeili, N.; Asadollahi, M. Polymeric Mixed Matrix Membranes Containing Zeolites as a Filler for Gas Separation Applications: A Review. *J. Ind. Eng. Chem.* **2013**, *19*, 375−393.
(7) Pechar, T. W.; Kim, S.; Vaughan, B.; Marand, E.; Tsapatsis, M.; Jeong, H. K.; Cornelius, C. J. Fabrication and Characterization of Polyimide−Zeolite L Mixed Matrix Membranes for Gas Separations. *J. Membr. Sci.* **2006**, *277*, 195−202.
(8) Ge, L.; Zhu, Z.; Rudolph, V. Enhanced Gas Permeability by Fabricating Functionalized Multi-walled Carbon Nanotubes and Polyethersulfone Nanocomposite Membrane. *Sep. Purif. Technol.* **2011**, *78*, 76−82.
(9) Ge, L.; Zhu, Z.; Li, F.; Liu, S.; Wang, L.; Tang, X.; Rudolph, V. Investigation of Gas Permeability in Carbon Nanotube (CNT)−Polymer Matrix Membranes via Modifying CNTs with Functional Groups/Metals and Controlling Modification Location. *J. Phys. Chem. C* **2011**, *115*, 6661−6670.
(10) Vu, D. Q.; Koros, W. J.; Miller, S. J. Mixed Matrix Membranes Using Carbon Molecular Sieves: I. Preparation and Experimental Results. *J. Membr. Sci.* **2003**, *211*, 311−334.
(11) Weng, T.-H.; Tseng, H.-H.; Wey, M.-Y. Fabrication and Characterization of Poly(phenylene oxide)/SBA-15/Carbon Molecule Sieve Multilayer Mixed Matrix Membrane for Gas Separation. *Int. J. Hydrogen Energy* **2010**, *35*, 6971−6983.
(12) Zornoza, B.; Irusta, S.; Téllez, C.; Coronas, J. N. Mesoporous Silica Sphere−Polysulfone Mixed Matrix Membranes for Gas Separation. *Langmuir* **2009**, *25*, 5903−5909.
(13) Yang, T.; Xiao, Y.; Chung, T.-S. Poly-/Metal-Benzimidazole Nano-Composite Membranes for Hydrogen Purification. *Energy Environ. Sci.* **2011**, *4*, 4171−4180.
(14) Adams, R.; Carson, C.; Ward, J.; Tannenbaum, R.; Koros, W. Metal Organic Framework Mixed Matrix Membranes for Gas Separations. *Microporous Mesoporous Mater.* **2010**, *131*, 13−20.
(15) Sumida, K.; Rogow, D. L.; Mason, J. A.; McDonald, T. M.; Bloch, E. D.; Herm, Z. R.; Bae, T. H.; Long, J. R. Carbon Dioxide Capture in Metal-Organic Frameworks. *Chem. Rev.* **2012**, *112*, 724−781.
(16) Jeazet, H. B. T.; Staudt, C.; Janiak, C. A Method for Increasing Permeability in O_2/N_2 Separation with Mixed-matrix Membranes Made of Water-Stable MIL-101 and Polysulfone. *Chem. Commun.* **2011**, *48*, 2140−2142.
(17) Ferey, G. Hybrid Porous Solids: Past, Present, Future. *Chem. Soc. Rev.* **2008**, *37*, 191−214.
(18) Li, J.-R.; Sculley, J.; Zhou, H.-C. Metal−Organic Frameworks for Separations. *Chem. Rev.* **2012**, *112*, 869−932.
(19) Perez, E. V.; Balkus, K. J., Jr.; Ferraris, J. P.; Musselman, I. H. Mixed-Matrix Membranes Containing MOF-5 for Gas Separations. *J. Membr. Sci.* **2009**, *328*, 165−173.

(20) Nik, O. G.; Chen, X. Y.; Kaliaguine, S. Functionalized Metal Organic Framework-Polyimide Mixed Matrix Membranes for CO_2/CH_4 Separation. *J. Membr. Sci.* **2012**, *413*, 48−61.
(21) Ren, H.; Jin, J.; Hu, J.; Liu, H. Affinity between Metal-Organic Frameworks and Polyimides in Asymmetric Mixed Matrix Membranes for Gas Separations. *Ind. Eng. Chem. Res.* **2012**, *51*, 10156−10164.
(22) Rodenas, T.; Van Dalen, M.; García-Pérez, E.; Serra-Crespo, P.; Zornoza, B.; Kapteijn, F.; Gascon, J. Visualizing MOF Mixed Matrix Membranes at the Nanoscale: Towards Structure-Performance Relationships in CO_2/CH_4 Separation Over NH_2-MIL-53(Al)@PI. *Adv. Funct. Mater.* **2014**, *24*, 249−256.
(23) Song, Q. L.; Nataraj, S. K.; Roussenova, M. V.; Tan, J. C.; Hughes, D. J.; Li, W.; Bourgoin, P.; Alam, M. A.; Cheetham, A. K.; Al-Muhtaseb, S. A.; Sivaniah, E. Zeolitic Imidazolate Framework (ZIF-8) Based Polymer Nanocomposite Membranes for Gas Separation. *Energy Environ. Sci.* **2012**, *5*, 8359−8369.
(24) Zhang, C.; Dai, Y.; Johnson, J. R.; Karvan, O.; Koros, W. J. High Performance ZIF-8/6FDA-DAM Mixed Matrix Membrane for Propylene/Propane Separations. *J. Membr. Sci.* **2012**, *389*, 34−42.
(25) Wijenayake, S. N.; Panapitiya, N. P.; Versteeg, S. H.; Nguyen, C. N.; Goel, S.; Balkus, K. J.; Musselman, I. H.; Ferraris, J. P. Surface Cross-Linking of ZIF-8/Polyimide Mixed Matrix Membranes (MMMs) for Gas Separation. *Ind. Eng. Chem. Res.* **2013**, *52*, 6991−7001.
(26) Askari, M.; Chung, T.-S. Natural Gas Purification and Olefin/Paraffin Separation Using Thermal Cross-Linkable Co-Polyimide/ZIF-8 Mixed Matrix Membranes. *J. Membr. Sci.* **2013**, *444*, 173−183.
(27) Ge, L.; Zhou, W.; Rudolph, V.; Zhu, Z. Mixed Matrix Membranes Incorporated with Size-Reduced Cu-BTC for Improved Gas Separation. *J. Mater. Chem. A* **2013**, *1*, 6350−6358.
(28) Shi, G. M.; Yang, T. X.; Chung, T. S. Polybenzimidazole (PBI)/Zeolitic Imidazolate Frameworks (ZIF-8) Mixed Matrix Membranes for Pervaporation Dehydration of Alcohols. *J. Membr. Sci.* **2012**, *415*, 577−586.
(29) Chen, X. Y.; Vinh-Thang, H.; Rodrigue, D.; Kaliaguine, S. Amine-Functionalized MIL-53 Metal-Organic Framework in Polyimide Mixed Matrix Membranes for CO_2/CH_4 Separation. *Ind. Eng. Chem. Res.* **2012**, *51*, 6895−6906.
(30) Perez, E. V.; Balkus, K. J., Jr.; Ferraris, J. P.; Musselman, I. H. Mixed-Matrix Membranes Containing MOF-5 for Gas Separations. *J. Membr. Sci.* **2009**, *328*, 165−173.
(31) Bae, T.-H.; Lee, J. S.; Qiu, W.; Koros, W. J.; Jones, C. W.; Nair, S. A High-Performance Gas-Separation Membrane Containing Submicrometer-Sized Metal−Organic Framework Crystals. *Angew. Chem. Int. Ed.* **2010**, *49*, 9863−9866.
(32) Kim, T. H.; Koros, W. J.; Husk, G. R.; O'Brien, K. C. Relationship between Gas Separation Properties and Chemical Structure in a Series of Aromatic Polyimides. *J. Membr. Sci.* **1988**, *37*, 45−62.
(33) Coleman, M. R.; Koros, W. J. Isomeric Polyimides Based on Fluorinated Dianhydrides and Diamines for Gas Separation Applications. *J. Membr. Sci.* **1990**, *50*, 285−297.
(34) Hou, L.; Shi, W. J.; Wang, Y. Y.; Guo, Y.; Jin, C.; Shi, Q. Z. A Rod Packing Microporous Metal-Organic Framework: Unprecedented ukv Topology, High Sorption Selectivity and Affinity for CO_2. *Chem. Commun.* **2011**, *47*, 5464−5466.
(35) Jiang, H.-L.; Lin, Q.-P.; Akita, T.; Liu, B.; Ohashi, H.; Oji, H.; Honma, T.; Takei, T.; Haruta, M.; Xu, Q. Ultrafine Gold Clusters Incorporated into a Metal−Organic Framework. *Chem.—Eur. J.* **2011**, *17*, 78−81.
(36) Ding, Y.; Bikson, B.; Nelson, J. K. Polyimide Membranes Derived from Poly(amic acid) Salt Precursor Polymers. 1. Synthesis and Characterization. *Macromolecules* **2001**, *35*, 905−911.
(37) Rallapalli, P.; Prasanth, K. P.; Patil, D.; Somani, R. S.; Jasra, R. V.; Bajaj, H. C. Sorption Studies of CO_2, CH_4, N_2, CO, O_2 and Ar on Nanoporous Aluminum Terephthalate [MIL-53(Al)]. *J. Porous Mater.* **2010**, *18*, 205−210.
(38) Rubal, M.; Wilkins, C. W.; Cassidy, P. E.; Lansford, C.; Yamada, Y. Fluorinated Polyimide Nanocomposites for CO_2/CH_4 Separation. *Polym. Adv. Technol.* **2008**, *19*, 1033−1039.
(39) Fang, X.; Xie, X. Q.; Simone, C. D.; Stevens, M. P.; Scola, D. A. A Solid-State ^{13}C NMR Study of the Cure of ^{13}C-Labeled Phenylethynyl End-Capped Polyimides. *Macromolecules* **2000**, *33*, 1671−1681.
(40) Grobelny, J.; Rice, D. M.; Karasz, F. E.; MacKnight, W. J. High-Resolution Solid-State Carbon-13 Nuclear Magnetic Resonance Study of Polybenzimidazole/Polyimide Blends. *Macromolecules* **1990**, *23*, 2139−2144.
(41) Ahn, J.; Chung, W.-J.; Pinnau, I.; Guiver, M. D. Polysulfone/Silica Nanoparticle Mixed-Matrix Membranes for Gas Separation. *J. Membr. Sci.* **2008**, *314*, 123−133.
(42) Aroon, M. A.; Ismail, A. F.; Matsuura, T.; Montazer-Rahmati, M. M. Performance Studies of Mixed Matrix Membranes for Gas Separation: A Review. *Sep. Purif. Technol.* **2010**, *75*, 229−242.
(43) Wijmans, J. G.; Baker, R. W. The Solution-Diffusion Model: A Review. *J. Membr. Sci.* **1995**, *107*, 1−21.
(44) Kanehashi, S.; Nagai, K. Analysis of Dual-Mode Model Parameters for Gas Sorption in Glassy Polymers. *J. Membr. Sci.* **2005**, *253*, 117−138.
(45) Merkel, T. C.; Freeman, B. D.; Spontak, R. J.; He, Z.; Pinnau, I.; Meakin, P.; Hill, A. Sorption, Transport, and Structural Evidence for Enhanced Free Volume in Poly(4-methyl-2-pentyne)/Fumed Silica Nanocomposite Membranes. *Chem. Mater.* **2003**, *15*, 109−123.
(46) Paul, D. R. Gas Sorption and Transport in Glassy Polymers. *Bunsen-Ges. Phys. Chem. Ber.* **1979**, *83*, 294−302.